JOURNAL OF GUIDANCE, CONTROL, AND DYNAMICS
Vol. 28, No. 1, January–February 2005

Integrated Design of the Motion Cueing System for a Wright Flyer Simulator

Ruud J. A. W. Hosman*
Aerospace Man–Machine Systems Consulting, 2645 KN Delfgauw, The Netherlands
Sunjoo K. Advani†
Aircraft Development and System Engineering, 2132 HB Hoofddorp, The Netherlands
and
Nils Haeck‡
3223 AH Hellevoetsluis, The Netherlands

Given a specific flight vehicle and a flying task—in this case, the 1903 Wright Flyer—a forward design process can be utilized to specify a corresponding flight simulator motion cueing system. This process, presented in this paper, is based on the analysis of the pilot–vehicle control loop by using a pilot model incorporating both visual and vestibular feedback and the aircraft dynamics. After substituting the pilot model to control the simulated aircraft, the analysis tools are used to adjust the washout filter parameters with the goal of maintaining the original pilot control behavior as much as possible. This process allows the objective specification of the motion cueing algorithm. Then, based on flight files representative of the operational flight envelope the required motion system work space is determined. The motion-base geometry is established based on practical limitations, as well as criteria for the stability of the platform with respect to singular conditions. With this process the characteristics of the aircraft, the tasks to be simulated, and the missions themselves are taken into account in defining the simulator motion cueing system.

Nomenclature

e	=	attitude error
g	=	gravity
H_c	=	controlled system
H_p	=	pilot transfer function
i	=	forcing function signal
J	=	cost function
Q, R	=	weighting factors
r	=	sensory output
u	=	pilot's control output
W	=	weighting factor
w	=	disturbance signal
wr	=	wing warp plus rudder interlink deflection
y	=	controlled system output
δ_c	=	canard deflection
θ	=	pitch angle
τ_i	=	information processing time delay
φ	=	roll angle
φ_m	=	phase margin
ω_c	=	crossover frequency
ω_n	=	natural frequency of the neuromotor system
ω_{sp}	=	short-period mode frequency

Subscripts

C, att	=	central visual system, attitude perception
C, rate	=	central visual system, rate perception
c	=	controlled system
Dist	=	disturbance task
I	=	information processing
Man	=	maneuver task
p	=	pilot
scc	=	semicircular canals
vest	=	vestibular
vis	=	visual

Presented as Paper 2002-4684 at the Integrated design of a motion cueing algorithm and motion-base mechanism for a Wright Flyer simulator, Monterey, CA, 5–8 August 2002; received 30 June 2003; revision received 28 November 2003; accepted for publication 3 December 2003.

*Director. Member AIAA.
†Director, Simulation and Training. Senior Member AIAA.
‡Mathematics and Motion Control Specialist.

Introduction

ORVILLE Wright, the pilot of the first engine-powered airplane, was faced with an exceptionally difficult task to manually control an unstable flight vehicle with no prior formal training in powered flight. He was purely reliant on his innate capacity to sense the vehicle motions, to visualize its flight path, and to adjust his control outputs to maintain a stable pilot–vehicle system. It was an unstable airplane, particularly in its pitch motions as both Orville and Wilbur quickly discovered, and required very careful manipulation of the forward rudder (as their canard was then referred to). Correction for the turbulence present at Kill Devil Hill that day made the task indeed a very challenging one.[1]

Since the first flights of the Wright brothers on 17 December 1903, both aerospace and simulation technologies have progressed hand-in-hand. Motion cueing systems have been utilized in simulators since the 1970s. When the motion cues produced by the motion systems are coupled with powerful visual display systems, the modern simulator can provide a powerful sensation of self-motion. However, even though today's civil aviation regulations require the presence of motion-cueing systems on high-end training simulators, there are yet no cueing criteria for motion-cueing systems.

The choice of motion system characteristics is based on the requirements of the simulator user and, if applicable, regulatory requirements. The major part of the motion system requirements, in particular the motion space, system bandwidth, maximum load, etc., are actually dependent upon the task to be simulated. The current lack of motion-cueing criteria, however, is the primary reason that there has been no real progress in the development of motion-cueing algorithms and the systematic design of simulator motion systems during the last decades. As a result, the final specifications are

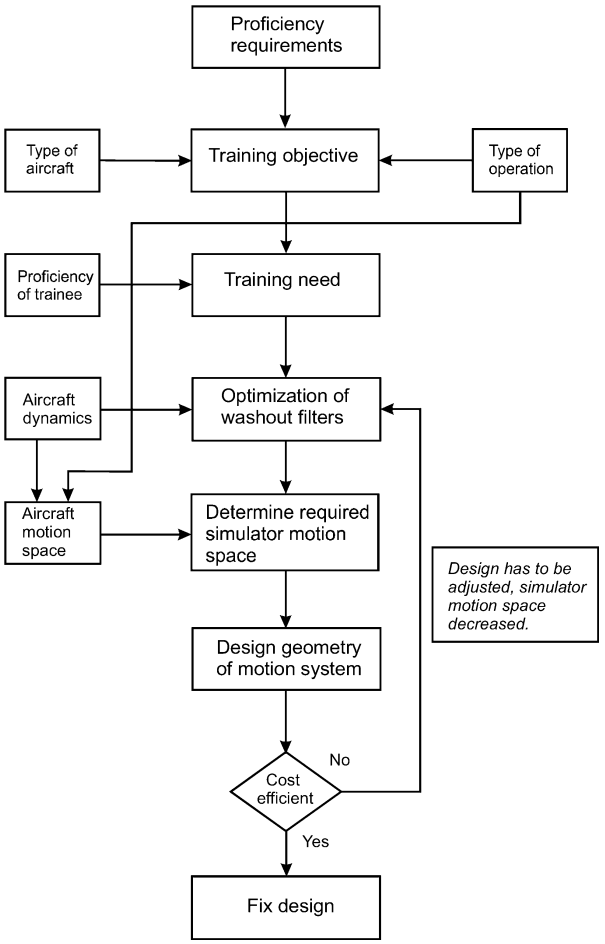

Fig. 1 Integrated motion-cueing system design process.

primarily based on emperical knowledge and experience, rather than the actual need.

Teunissen[2] suggests that for the selection of the training means from computer-based trainer to full flight simulator (FFS) it is necessary to first specify the training objective (the level of proficiency that the trainee has to master) and the training need (the difference between the objective and the proficiency before the training). If the selection of the FFS is based on such a specification, then the motion cueing characteristics must still be defined. It is known that the flight maneuvers to be simulated, and the properties of the motion cueing algorithm, determine the required motion space of the motion system.

In an effort to overcome this status quo, Advani and Hosman[3] presented in 2000 a scheme for an integrated design of the motion-cueing algorithm and the motion system (Fig. 1). Based on this strategy, both the motion-cueing algorithm (also known as the wash-out filter) and the motion system geometry can be specified if the required knowledge, information, and software are available.

Since 2000, several customers have shown interest in the integrated design method. Several projects to design these wash-out filters, the motion system geometry,[4] and the combined integrated design of the motion system and wash-out algorithm[5] have been performed since[3] or are currently in progress.

The present paper will discuss the details, merits, and shortcomings of this design procedure, based on an example employing the 1903 Wright Flyer. First an overview of the process and its building blocks will be presented. Thereafter, the results are shown and discussed and conclusions drawn.

Simulator Motion-Cueing System Design Process and Elements

The authors have developed a systematic means of specifying simulator motion-cueing systems, incorporating the motion drive algorithm and the motion-base mechanism (Fig. 1). The design process follows four essential steps:

1) Adjust a validated pilot model[6,7] to the given dynamics of the aircraft.

2) Introduce simulator parameters (time delays and the wash-out filter form), and adjust the wash-out algorithm parameters in order to maintain the pilot's control behavior in the simulation as closely as possible to that in the aircraft.

3) Based on recorded flight trajectories (real or simulated) representative for the aircraft operation and the optimized wash-out algorithm, generate simulator motion system trajectories

4) Design a simulator motion base that contains these trajectories as best as possible.

The integrated design is based on a sequential analysis, which leads to the optimization of the motion-cueing algorithm and the geometry of the motion system. For the analysis, the following models are required: 1) an aerodynamic model of the aircraft, 2) a model describing a pilot's skill-based control behavior incorporating the visual and vestibular feedback, 3) a model describing a pilot's motion perception incorporating visual and vestibular stimulation, 4) a model describing the general form of the motion-cueing algorithm, 5) a set of (simulated) flight files covering the operation to be simulated, and 6) a tool to optimize the design of the motion system, including a means of comparing the actual available work-space with that required by the preceding simulations. In the Wright Flyer example discussed in this paper, linear models will be used. This is not a requisite, but for the analysis based on nonlinear models more detailed information and knowledge would be required, and the analysis itself is much more extensive. Both the aircraft model and the flight files were provided from the University of Liverpool. The flight trajectory files were generated during a generic piloted moving-base simulation of the Wright Flyer.

As described by Hosman,[8] a distinction must be made regarding the influence of motion feedback at each of the three different levels of behavior as described by Rasmussen.[9] These levels are skill-based (manual control), rule-based, and knowledge-based behavior.

Pilot-Model Adaptation to the Aircraft Model

The first step required for this analysis is to adapt the pilot model to the aircraft dynamics in the attitude control loop (Fig. 2). In this figure two external sources influencing the closed loop, $i(t)$ and $w(t)$, are shown. The pilot model used in this type of analysis must be able to process the contribution of the visual and vestibular feedback[6,7,10] in the inner attitude control loop on the pilot's skill-based manual control behavior. Based on extensive research on the influence of visual and vestibular perception of motion stimuli and on motion perception and control behavior in tracking tasks, a descriptive pilot model has been developed and validated.[6,7] The aim

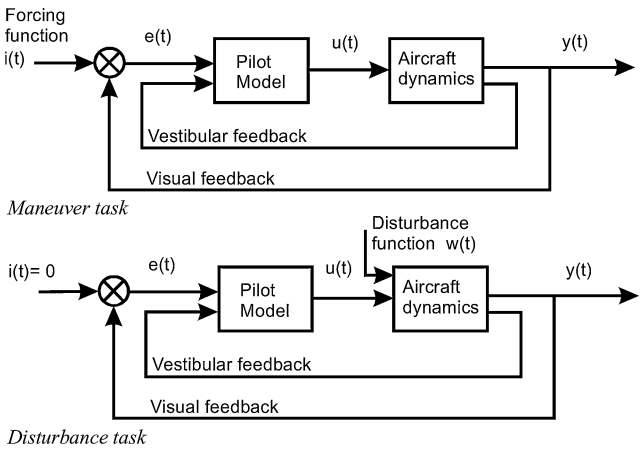

Fig. 2 Closed loop with the pilot and the aircraft with the visual and the vestibular feedback loops. A distinction between the maneuver task and the disturbance task is made depending on the external sources $i(t)$ and $w(t)$ influencing the control loop.

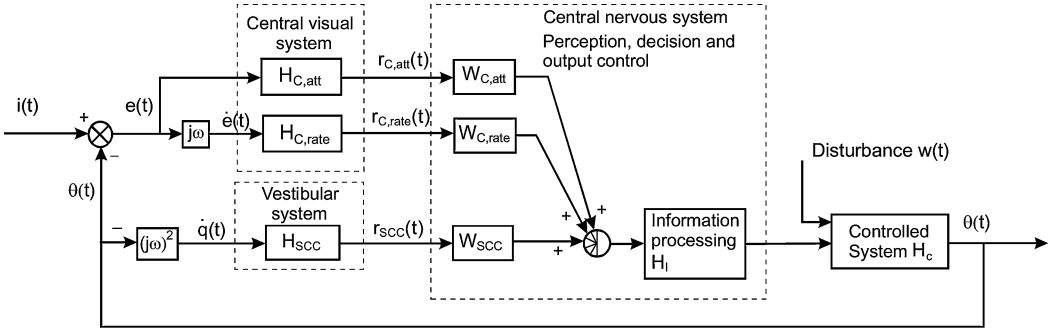

Fig. 3 Block diagram of the descriptive pilot model. Note that the output of the controlled system, the aircraft, is attitude and that a differentiator and a double differentiator is required to derive the proper input for the representations of the visual rate perception $H_{C,\text{rate}}$ and the semicircular canals H_{SCC}.

was to attain a model capable of describing the influence of the visual and vestibular stimulation induced by the aircraft motions on a pilot's control behavior. The final model is depicted in Fig. 3.

With the experiments described by Hosman,[6,7,11] the dynamics of the sensors and the interaction between the visual and the vestibular systems were evaluated. In this model, the human motion sensors—each of which is described by a transfer function—are placed in parallel and convert the stimuli (the attitude, angular rate, and angular acceleration) to the sensory outputs $\omega r_I(t)$. The differences in sensor dynamics are caused by the fundamental differences between the visual and the vestibular system: The visual system is position sensitive and generates rate by the bilocal motion detector in the visual cortex.[6] The vestibular system is sensitive to angular accelerations and specific forces. The semicircular canals are sensitive to angular acceleration, whereas the otoliths are sensitive to specific force.

In the perception and decision process, the many sensory outputs have to be integrated into one single output. Based on the experimental results during tracking tasks, the model output is generated by a weighted sum of the sensory outputs. Each individual weighting factor W_i emphasizes the contribution of each sensory output.

Next, the time delay resulting from the information processing and a simulation of the total neuromuscular-manipulator control system are incorporated into the model.

Because of the high-bandwidth character of a well-designed neuromotor-manipulator control system ($\omega_n \gg \omega_c$), the information processing delay and the neuromotor-manipulator system can be modeled by one single lumped time delay τ_I. Taking into consideration the effective time delay of the human operator in tracking tasks,[12] and the characteristics of the visual system, Hosman[6] and Hosman and Stassen[7] initially set $\tau_I = 0.2$ s to simultaneously represent the information processing time delay and the neuromuscular dynamics. This value is valid for tracking tasks with a side stick as the manipulator and system dynamics that allow a high closed-loop bandwidth ($\omega_c > 3$ rad/s). For system dynamics corresponding with those of transport aircraft, a time delay and neuromuscular dynamics (that account for the influence of the aircraft control system, columb, or wheel) have to be incorporated within the pilot model.

When a pilot adjusts his/her behavior to a certain control task, the first objective is to achieve an acceptable level of tracking performance. Normally, this tracking performance can be quantified by the mean square of the tracking error. When the pilot would try to minimize the tracking error alone, his control actions would not be taking into account the aircraft characteristics, structural loads, and passenger comfort, for example. Therefore, if the mean square error were the only component of the cost function used to adapt the model to the aircraft dynamics this would drive the model parameters to a value for best performance regardless of the effect on the dynamic characteristics of the closed loop. In reality, the pilot will normally consider putting more effort into the task as a function of the benefit of the resulting performance improvement and the corresponding increase in workload.

There is another consideration: When a pilot tries to improve tracking performance, he will also increase his gain. This will result in an increase of the crossover frequency ω_c and a decrease in phase margin φ_m. For transport aircraft the crossover frequency has to be lower than the natural frequency of the particular mode to be controlled, that is, the short-period and the roll mode. A gain that is too high will reduce the stability of the control loop. So, the choice of the cost function should aim at the following: 1) good tracking *performance*, 2) effective control *effort*, and 3) adequate *bandwidth* and *stability* of the control loop as expressed in the crossover frequency and in the phase margin. For these reasons, the mean square of the control signal δ and its derivative $\dot{\delta}$ have to be added to the cost function.

To achieve these goals, the following cost function will be applied:

$$J = \Sigma(e^2 + Q \cdot u^2 + R \cdot \dot{u}^2) \tag{1}$$

Q and R in the cost function depend primarily on the aircraft characteristics and on the task to be performed, that is, the disturbance or maneuver task.

Task Dependence

With this model, the influence of visual and vestibular motion feedback in both the maneuver task and the disturbance task can be described. The advantage of the model is that by describing the influence of the visual and vestibular feedback on a pilot's control behavior; the only free model parameters are the sensory weighting coefficients W_i, as shown in Fig. 3.

In Fig. 2 two control loops are shown. In the first one, the maneuver task, pilot's control is directed to minimize the attitude error $e(t)$ when making the aircraft following the external reference or forcing function. In the second, the disturbance task, pilot's control is aimed at minimizing the attitude error $e(t)$ caused by the external disturbance as turbulence. These two tasks have a different influence on pilot's control behavior. This difference is enhanced by motion feedback.[13] The transfer function describing pilot's control behavior is defined as

$$H_p(\omega) = U(\omega)/E(\omega) \tag{2}$$

Depending on the task, maneuver task vs disturbance task, the transfer function can be derived as follows: In Fig. 4 the pilot model of Fig. 3 with the visual and vestibular feedback is simplified to two transfer functions $H_{p,\text{vis}}(\omega)$ and $H_{p,\text{vest}}(\omega)$. In this figure $y(t)$ is the aircraft attitude. In the maneuver task the attitude error $e(t) = i(t) - y(t)$, whereas in the disturbance task $e(t) = -y(t)$.

In the case of the maneuver task, the motion feedback forms an additional feedback loop, which leads to

$$H_{p,\text{Man}}(\omega) = \frac{H_{p,\text{vis}}(\omega)}{1 + (j\omega)^2 H_{p,\text{vest}}(\omega) H_c(\omega)} \tag{3}$$

For the disturbance task $H_{p,\text{vis}}(\omega)$ and $H_{p,\text{vest}}(\omega)$ contribute to the control output in paralel. Hence the control behavior is described by

$$H_{p,\text{Dist}}(\omega) = H_{p,\text{vis}}(\omega) + (j\omega)^2 H_{p,\text{vest}}(\omega) \tag{4}$$

When these transfer function are worked out for the full pilot model of Fig. 3, then the following transfer functions for pilot's control behavior in the maneuver and disturbance task can be derived:

$$H_{p,\mathrm{Man}}(\omega) = \frac{[W_{C,\mathrm{att}} \cdot H_{C,\mathrm{att}}(\omega) + W_{C,\mathrm{rate}} \cdot H_{C,\mathrm{rate}}(\omega) \cdot j\omega]}{\left[1 + W_{\mathrm{SCC}} \cdot H_{\mathrm{SCC}}(\omega) \cdot (j\omega)^2 \cdot H_i(\omega) \cdot H_c(\omega)\right]} \cdot H_i(\omega) \tag{5}$$

and

$$H_{p,\mathrm{Dist}}(\omega) = \left[W_{C,\mathrm{att}} \cdot H_{C,\mathrm{att}}(\omega) + W_{C,\mathrm{rate}} \cdot H_{C,\mathrm{rate}}(\omega) \cdot j\omega + W_{\mathrm{SCC}} \cdot H_{\mathrm{SCC}}(\omega) \cdot (j\omega)^2\right] \cdot H_i(\omega) \tag{6}$$

The cost function of Eq. (1) will be used to adjust the descriptive pilot model to the dynamics of the aircraft. To prevent the adjustment to a minimum of the cost function outside the normal operation area of the pilot, additional constrains can be required in order to attain a practical and sound result of the optimization.

Motion Wash-Out Parameter Adjustment

After the pilot model has been adapted to the particular aircraft dynamics, the closed loop of Fig. 2 is adapted to the closed loop of the simulated aircraft (Fig. 5). In this scheme, three elements are added to the pilot–aircraft control loop: a lumped simulation time delay, the wash-out filter, and the motion system. In the present analysis, it is first assumed that the motion system behaves perfectly in terms of its dynamics and has a gain of one. This assumption is made because the dimensions of the motion system are not yet known and a correction for the dynamics can be applied.

Because of the changes of the control loop as caused by the simulation, the pilot will adapt his behavior to the simulated-aircraft control loop. Using the pilot and aircraft model as the basis, the wash-out algorithm parameters are adjusted by hypothesizing that the cost function used to adapt the pilot model to the aircraft dynamics indeed describes the pilot's control strategy.

In the end, the motion wash-out algorithm coefficients remain the *only* parameters that can be adjusted in this phase. When the transfer function of these algorithms is introduced into the pilot–vehicle system, their coefficients can be adjusted then through a optimization procedure. In the end, the optimization should restore the pilot control behavior as closely as possible to the original behavior. This is accomplished by using the same weighing factors in the cost function J [see Eq. (1)], in finding the optimal wash-out parameters. The resulting control strategy by the pilot can then be maintained in the simulator as it originally was in the aircraft.

For the adaptation of the wash-out filters to the pilot model and aircraft dynamics in the present project, the following arguments have been applied: For a pilot's skill-based control behavior, the inner attitude control loops are of direct importance.[14] Therefore, the simulation of the pitch angle θ and the roll angle φ are of primary interest. When applying the classical wash-out filter, the high-pass rotational filter and the low-pass tilt-coordination filters generate the pitch and roll angles. The high-frequency components pass through the high-pass filter. The low-frequency components pass through the gravity component $g \sin\theta$ or $g \sin\varphi \cos\theta$ of the specific force and are filtered by the tilt-coordination filter. Therefore, the wash-out filter's influence on the simulated aircraft pitch attitude can be simplified, as shown in Fig. 6. For the roll attitude, the lateral specific force is zero in a coordinated maneuver, and the simulator roll angle results from the high-pass rotation filter.

The remaining wash-out filter parameters, namely, the high-pass translational filters, have a direct influence on a pilot's rule-based and knowledge-based behavior. For these levels of behavior, the perception of the aircraft motions in the environment directly impacts the performance. A *general* motion perception model is required in order to analyze and optimize the translational filters. Such a motion perception model is under development at TNO-Human Factors Institute in Soesterberg, the Netherlands. Bos et al.[15] applied this model to the motion perception during the takeoff run of a transport aircraft. Although further development and evaluation are required, this model can be applied to the optimization of the translational filters in the wash-out algorithm. Therefore, in the present analysis

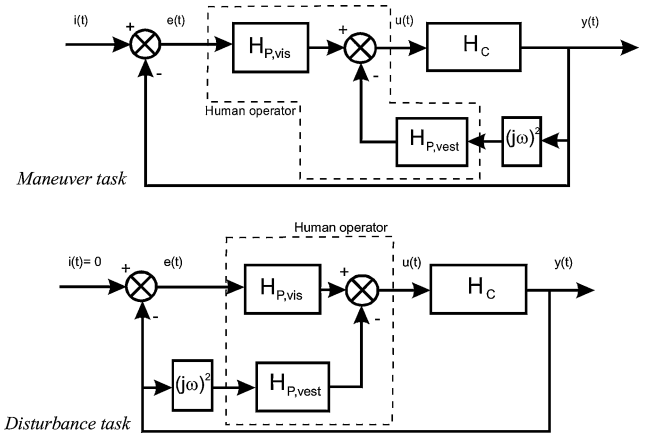

Fig. 4 Simplified schemes of the pilot model in the closed loop for the maneuver task and the disturbance task.

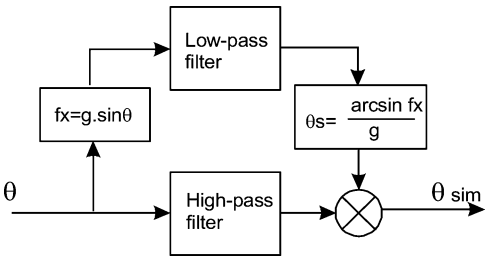

Fig. 6 Simplified schemes of the wash-out influence on the simulation of the pitch angle.

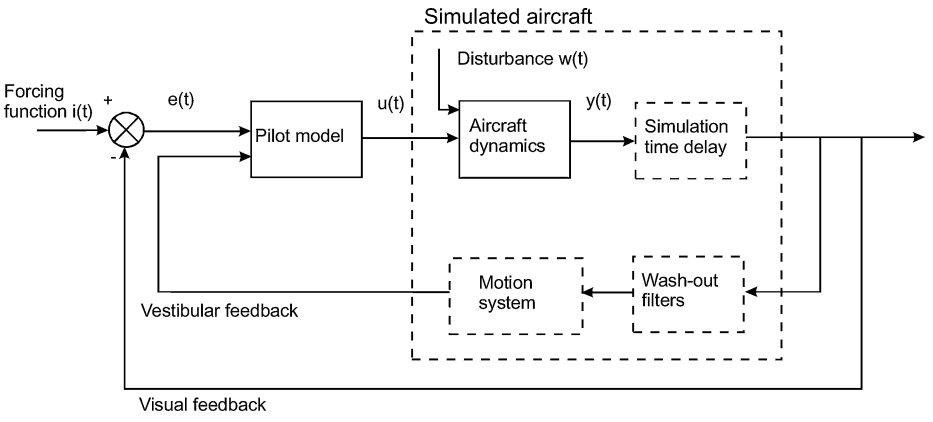

Fig. 5 Pilot simulated-aircraft control loop.

the translational filter parameters have to be chosen based on the authors' experience.

In the end, this step generates the required motion drive algorithm parameters in order that the pilot perceives and responds to the simulated vehicle in a way that is as similar as possible to the vehicle. Once the wash-out algorithm has been established, the required motion space can be determined.

Required Simulator Motion Envelope

To define objectively the six-degrees-of-freedom motion space that is required, measured state variables of an aircraft are passed through the motion drive algorithm in order to generate the ideal simulator trajectories. If the drive algorithm has been adjusted to the task and aircraft as just reported, and the maneuvers are measured under similar flight conditions with the same or similar aircraft, then a simulator that reproduces these trajectories should generate a perception and control output by the pilot just like in the aircraft. This is the basis of the remainder of this strategy.

Mechanism Design

The performance capability of a motion cueing system can be characterized by its kinematic envelope (or work space) and its dynamic characteristics, such as phase delay and damping. The latter are a function of the mechanical power available to move the moving platform, its mass properties, and its bandwidth. The motion work space is, however, a direct function of the architecture of the motion cueing mechanism.

Modern flight simulator motion bases generally utilize a mechanism known as the Stewart Platform,[16] or "hexapod," which was originally proposed in 1938 for the testing of vehicle tires. This mechanism is comprised of a base frame, six actuator legs (the jacks), and an upper moving platform, which carries the payload. The legs are attached in pairs, via gimbal joints, to the upper and lower platforms near the vertices of their respective triangular frames (Fig. 7).

The kinematic envelope (work space) of a hexapod is limited and highly coupled. For example, a pitch-up attitude of 20 deg (common during the simulation of a takeoff) will reduce the available motions in all other directions and rotations to nearly zero.

A typical hexapod is symmetric along three axes at increments of 120 deg. For flight simulation, symmetry about the X-Z plane is important, and the motion envelope can also be tailored to the specific requirements of the simulation. It is technically feasible to change the layout of the hexapod (thereby deviating from the standard circular geometric arrangement of the attachment points) in order to achieve a greater and better distribution of the workspace.[17,18]

For example, one can theoretically place the hinge points (gimbals) anywhere in space such as on two concentric, noncoplanar circles,[17] rather than on one circle (Fig. 8).

It is also easy for some manufacturers to change the cut length of the actuator cylinders and piston rods, while maintaining the original design of the hinge forks, manifolds, cushioning buffers,

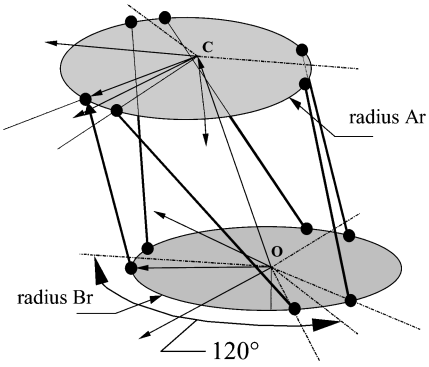

Fig. 7 Kinematic representation of the typical circular layout Stewart Platform (hexapod) mechanism.

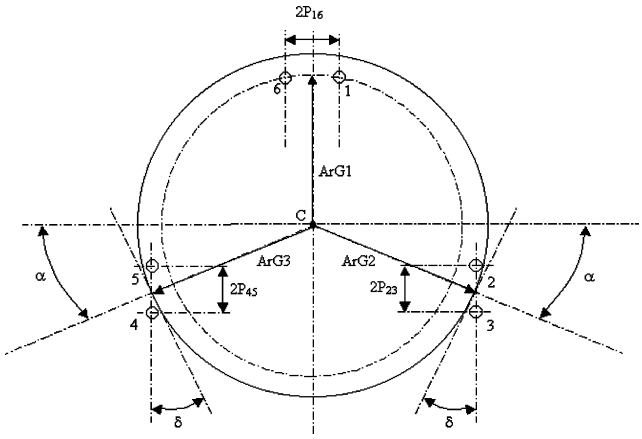

Fig. 8 Layout of double-concentric platform.

and end blocks. The actuator stroke length can also be specified by the design requirements (rather than arbitrarily chosen multiples of prime numbers, as is often the case).

However, the designer must also prevent the platform from ever approaching singular conditions. In this situation, the ratio of actuator displacements to the resulting platform displacements is very low, meaning that the positioning accuracy can suffer, the mechanical loads can become high, or the control of the system can be difficult to achieve.

By using an optimization program, all of the preceding free design variables and constraints can be combined to yield the most suitable architecture tailored to the specified motion envelope.

A method of optimizing the motion base,[17,18] based on the following steps, was developed and tested. The original reference[17] provides more details. The salient points are explained here:

1) Use the basic concept of the Stewart Platform.

2) Establish which geometric parameters should be allowed to vary and by how much and which should remain fixed.

3) Fit the shape and size of these required motions (as developed earlier in this article) into the available simulator motions by altering its geometry. This is accomplished through a mathematical optimization.

4) Check that the leg forces are within reasonable limits, that the legs do not exceed their minimum or maximum lengths, and that the legs do not make physical contact with each other.

5) Iterate when necessary.

To simplify the process of mathematical optimization, the six-dimensional trajectories were approximated by a single six-dimensional hyperellipsoid. This hyperellipsoid circumscribes the trajectories and serves as a weighting function of the platform motions in its six degrees of freedom. In step 3, these ellipses are inserted into the work space of the mechanism, and this work space is grown to allow the larges possible ellipse to be just contained within its space.[4,17] Increasing the work space and changing its relative shape are made possible by relocating the hinge points and, if necessary, changing the characteristics of the actuators, namely, their cut lengths.

Example: Integrated Design of an Optimum Wright Flyer Simulator Motion Cueing System and Motion-Base Mechanism

Aircraft Model

For this analysis, a linear model approximation of Wright Flyer dynamics has been used. Culick[19] analyzed the flight characteristics of the Wright Flyer and confirmed that the aircraft was indeed longitudinally and laterally unstable. For the longitudinal mode, the short-period mode is unstable, whereas for the lateral mode it is the spiral mode that is heavily unstable. From the linear state-space model the transfer functions for pitch attitude and roll attitude control were derived [Eq. (7)]. This model was received from the University of Liverpool, United Kingdom,[20] and corresponds quite

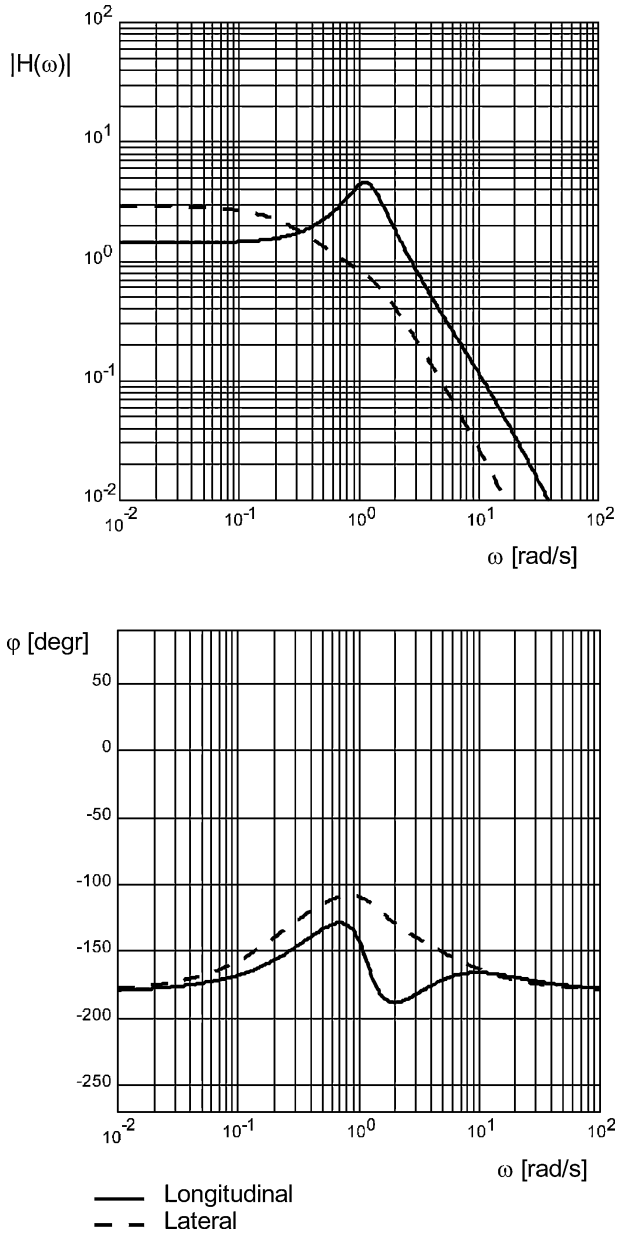

Fig. 9 Bode plot of the linear aircraft model.

well with that published by Jex et al.[21]

$$H\frac{\theta}{\delta_c}(s) = \frac{(15.0941s^2 + 71.6512s + 32.3732)}{(s^4 + 9.113s^3 - 8.261s^2 - 1.2524s - 22.6527)}$$

and

$$H\frac{\varphi}{wr}(s) = \frac{(2.8655s^2 + 6.444s + 5.4659)}{(s^4 + 5.3422s^3 + 7.2947s^2 + 5.7702s - 1.8952)} \tag{7}$$

The bode plots of these transfer functions are presented in Fig. 9.

Pilot-Model Adaptation

For the pilot-model adaptation, the sensory weighting coefficients W_i of Fig. 2 must now be chosen. This is accomplished through an optimization procedure using the cost function of Eq. (1). The Bode plot of the adapted pilot model with and without motion feedback in the disturbance task is presented in Fig. 10. Table 1 presents the model adjustment and closed-loop performance.

It is likely that the 1902 glider and 1903 Flyer both had overbalanced canards meaning that any deflection from the neutral position meant that the resulting airloads would tend to increase the deflection. The Wright Flyer pilot had not only to stabilize the control of the aircraft but also that of the canards with his neuromuscular system. To take that into account, the information processing time delay of $\tau = 0.2$ s (Fig. 3), was replaced by a small time delay ($\tau = 0.08$ s) together with a second-order system ($\omega = 9$ rad/s and $\zeta = 0.7$) to describe the neuromotor system dynamics.

To adjust the pilot model to the aircraft dynamics, it turned out that for pitch control the crossover frequency has to be increased above the natural frequency of the short period mode $\omega_{sp} = 1.181$ rad/s and that motion feedback is crucial to obtain enough phase margin, or stability. A crossover frequency $\omega_c = 3.1$ rad/s is not uncommon for the disturbance task with double integrator dynamics to control which dynamics are quite close to those of the Wright Flyer pitch dynamics.

From Table 1, it is clear that during the disturbance task the pilot model primarily uses vestibular feedback and that the phase margin for pitch control is small. In the maneuver task, it is the visual rate feedback that serves as the primary variable. In the case of the Wright Flyer, however, there is no such clear preference (for either visual or for vestibular motion feedback) during the maneuver task.

Table 1 Pilot model adjustment and loop closure results for longitudinal and lateral control, disturbance task, and maneuver task, and for visual only, visual and motion (real flight), simulated flight with CW2 classical wash-out filter,[17] and optimal wash out

Task	$W_{C,\text{att}}$	$W_{C,\text{rate}}$	W_{SCC}	Std error, deg	ω_c, rad/s	φ_m, deg
Disturbance						
		Pitch				
Visual only	0.750	0.330	0	4.961	3.550	14.2
Visual and motion	1.049	0.023	0.493	3.100	3.718	40.67
CW2 washout	0.850	0	0.450	4.695	4.294	15.35
Opt. washout	0.883	0	0.549	4.332	3.475	29.27
		Roll				
Visual only	1.342	0.395	——	1.478	1.366	65.07
Visual and motion	1.832	0	0.752	1.102	1.614	74.59
CW2 washout	1.656	0	0.449	1.265	1.388	74.04
Opt. washout	1.717	0	0.787	1.196	1.529	66.74
Maneuver						
		Pitch				
Visual only	0.100	0.273	——	2.116	2.097	30.79
Visual and motion	1.600	0.173	0.676	1.517	2.536	49.69
CW2 washout	1.390	0	1.100	1.886	1.897	55.65
Opt. washout	1.550	0.040	0.800	1.609	2.373	40.61
		Roll				
Visual only	1.482	0.528	0	1.242	1.617	62.41
Visual and motion	5.279	0	2.809	1.160	1.366	63.55
CW2 washout	2.312	0.290	0.666	1.317	1.106	63.33
Opt. washout	3.128	0.195	1.803	1.273	1.216	67.37

Wash-Out Algorithm Parameter Optimization

After the pilot model has been adapted to the aircraft dynamics, the pilot model parameters are fixed, and the pilot simulated-aircraft loop is established (Fig. 10). The wash-out filter parameters are optimized for the simulation of the Wright Flyer with a lumped simulation time delay of 70 ms present. Next, the parameters of the tilt-coordination filter and the high-pass rotation filter can be adapted using the cost function J of Eq. (1). In Fig. 11, as an example, the cost function is shown with respect to the tilt-coordination and rotation filter bandwidth $\omega_n(Lp)$ and $\omega_n(Hp)$, respectively. In most cases, the cost function J can be described by a valley as a function of the break frequencies of the high-pass rotational filter and the low-pass tilt-coordination filter. After the wash-out parameters have been established, the pilot model can be adapted to the simulated aircraft, and, subsequently, the pilot model adaptation to the real and the simulated aircraft compared. Figure 10 presents the pilot model in the frequency domain for the real aircraft 1) without and 2) with motion feedback, 3) the optimized washout filters as described in this paper,

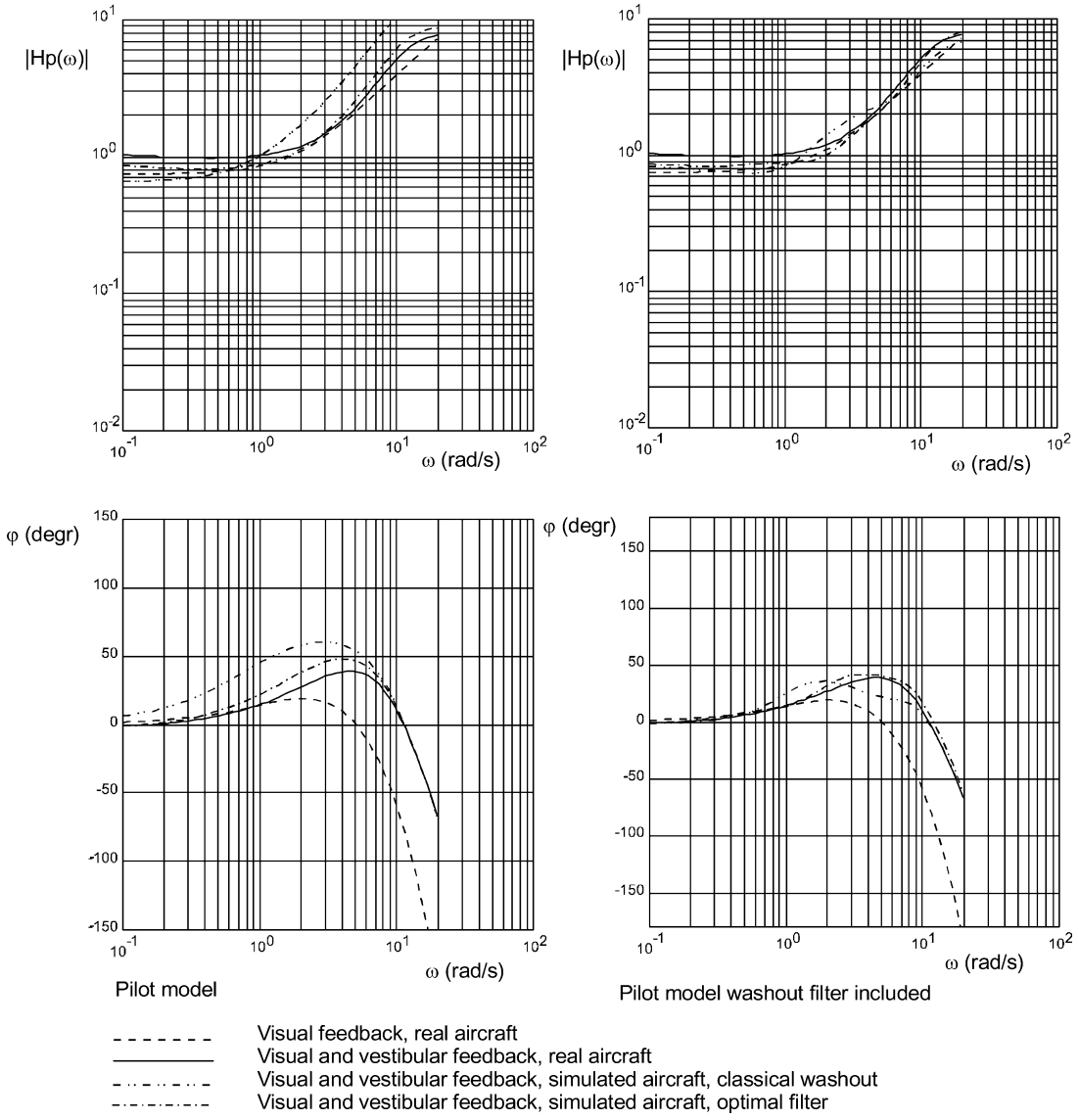

Fig. 10 Bode plot of the pilot model for the Wright Flyer with and without motion feedback and for the simulated aircraft with the influence of the classical wash-out filter and the optimal filter.

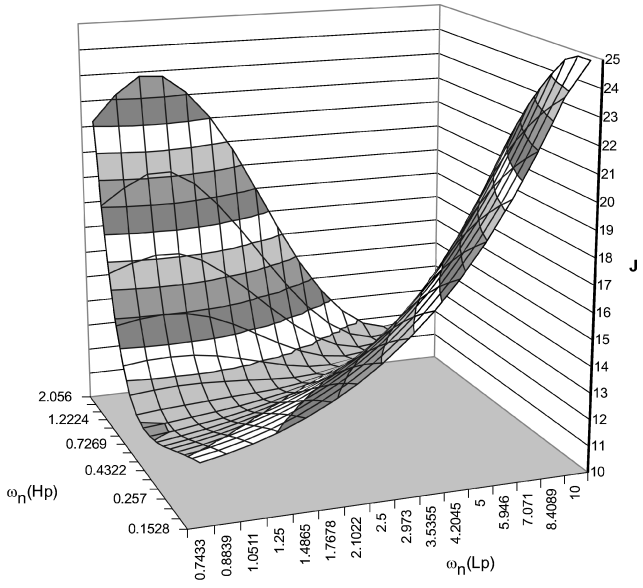

Fig. 11 Cost function J as a function of the bandwidth of the tilt-coordination filter $\omega_n(Lp)$ and the rotation filter $\omega_n(Hp)$ for the roll disturbance task.

and 4) a classical wash-out filter[22] as often used for transport aircraft training.

Realizing the Motion-Base Requirements

As mentioned earlier, the motion-base mechanism can be designed to fit trajectories representing the desired simulated motions. When a mechanism is able to reproduce these trajectories with no further gain distortion, no saturation of its actuators, and no phase lags beyond those used in the pilot-model based analysis, then the pilot control strategy should remain the same in the simulator as in the aircraft.

Obtaining representative trajectory data, however, requires either flight recordings or that the mathematical model of the aircraft be driven in the time domain. For obvious reasons, the latter was chosen in this case, making use of a research flight simulator at the University of Liverpool, which has a fully integrated model of the Wright Flyer coupled with flight controls and cueing devices.

The aircraft accelerations were registered during five representative maneuvers, and these later processed to generate the desired trajectories of the simulator. The positions and orientations, as well as their first and second derivatives, are thereby defined. The requirements of the motion base—at least for the reproduction of these specific cases—are fully resident then in this trajectory data.

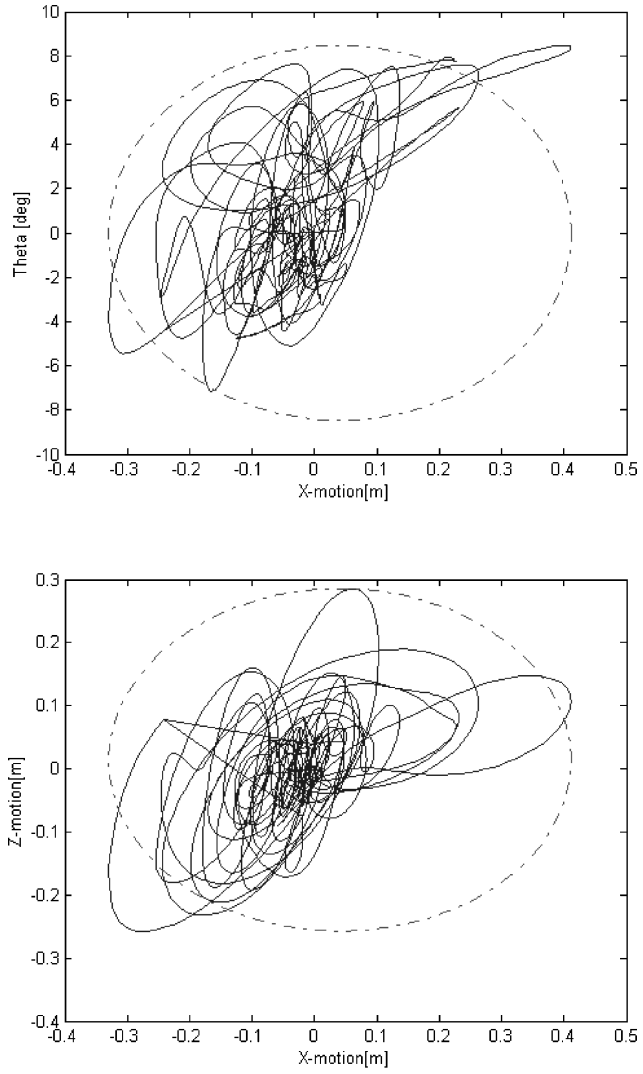

Fig. 12 Examples of the trajectories of the simulator motion system as a result of the flight files of the Wright Flyer and transformed by the optimal wash-out filter.

The trajectories are then encapsulated into a reasonable mathematical approximation, represented by a six-dimensional hyperellipsoid. If this ellipsoid contains these trajectories, and if it is possible to manufacture a motion system that is capable of generating a motion envelope at least as large as that ellipsoid, then it can be postulated that it is indeed possible to achieve our simulation needs.

Figure 12 shows the trajectories generated by the simulation of the 1903 Wright Flyer after they were passed through the optimized motion drive algorithm. In total, there are 15 combinations possible (e.g., surge-heave, surge-sway, heave-sway, pitch-roll, pitch-sway, pitch-yaw, pitch-surge, etc.), though we have shown only four for clarity. Note that symmetry is applied to all lateral motions in order to allow the resulting simulator specification to reflect the symmetric capabilities of the aircraft. (Motions to the left or to the right should be possible with equality.)

Furthermore, the ellipses shown in Fig. 12 are not centered about the origin. This allows the use of prepositioning (moving the motion base to a nonzero starting position) in anticipation of the motions that could be created during the simulated flight. Note that if the ellipses are centered, there is a chance that the size of the ellipse must be larger in order to contain the trajectories. Prepositioning is only relevant in the longitudinal translations (X and Z). The hyperellipsoid has also been generated for these motions and can also be seen in Fig. 12. The size of this ellipsoid is mathematically determined

Table 2 Hyperellipsoid weighting factors generated by analysis for the Wright Flyer example

Degree of freedom	Weighting factor
X	±0.370 m
Y	±0.140 m
Z	±0.674 m
Ψ	±4.2 deg
Θ	±8.46 deg
Φ	±8.47 deg

so that the lengths of the primary axes represent the projections of the trajectories along the direction of that axis. In other words, the hyperellipsoid indicates the relative weightings for each of the six degrees of freedom. If the trajectories include a large amount of cross coupling, then they will exceed the boundaries of the hyperellipsoid. This issue will be resolved in the next section on mechanism design.

Figure 12 also shows that the ellipsoid is not necessarily centered about the zero point in the X and Z degrees of freedom. In this figure, the origin represents the midpoint of the simulator motion-base neutral pose. The maneuvers and resulting trajectories dictate this offset, and one might need to preposition the simulator prior to a mission or maneuvers in order to allow its simulation without hitting the actuator travel limits and without having to overspecify the size of the motion-base.

Table 2 provides the weighting factors of the motions in each degree of freedom, which were generated by the optimal wash-out algorithm and trajectory approximation by the hyperellipsoid. Note that the trajectories also provide knowledge of the minimum required velocity and accelerations of the motion base.

Motion-Base Design

A tailored motion-base mechanism can now be designed to suit the requirements just generated. The parameters of the hexapod, as described in Fig. 8, were optimized in order to contain the resultant hyperellipsoid of Table 2. To demonstrate the effectiveness of the optimization, the geometric parameters of a very small commercially available hexapod with actuators having a total stroke length of 20 cm were used. The workspace of the system was reshaped to accommodate the requirement, in this case by changing only the locations of the attachment points. The actuator stroke length was maintained at 20 cm. Most importantly, although minor, the changes to the geometry ensure that the shape is tailored to the simulation need, based on the pilot model, the vehicle dynamics, and the maneuvers that are flown.

The workspace and general layout of the final system is shown in Fig. 13. Note that the vertical location of the lower joints is not coplanar, which allows more optimization freedom. It does mean though that the forward joints are located lower on the platform than the aft sets. The objective function increased from 0.332 to 0.430, and the shape of the work space became very conformant to that required, with little "wasted" capability. Note that these results show *one* possible solution; the actual design effort would yield several options because of the presence of many local minima, each of which represents a specific improvement in the work space and having a specific geometry. The designer must then choose the most viable outcome based, for example, on manufacturing cost and interface with the building or simulator structure.

Following this initial design step, a complete dynamics analysis is required during which the simulated mechanism is exercised throughout its envelope, and the loads in all members are checked. These verifications must include failure modes, such as runaway conditions and valve-0 conditions. Although these analyses have been performed for systems optimized by the authors, their description exceeds the scope of this paper.

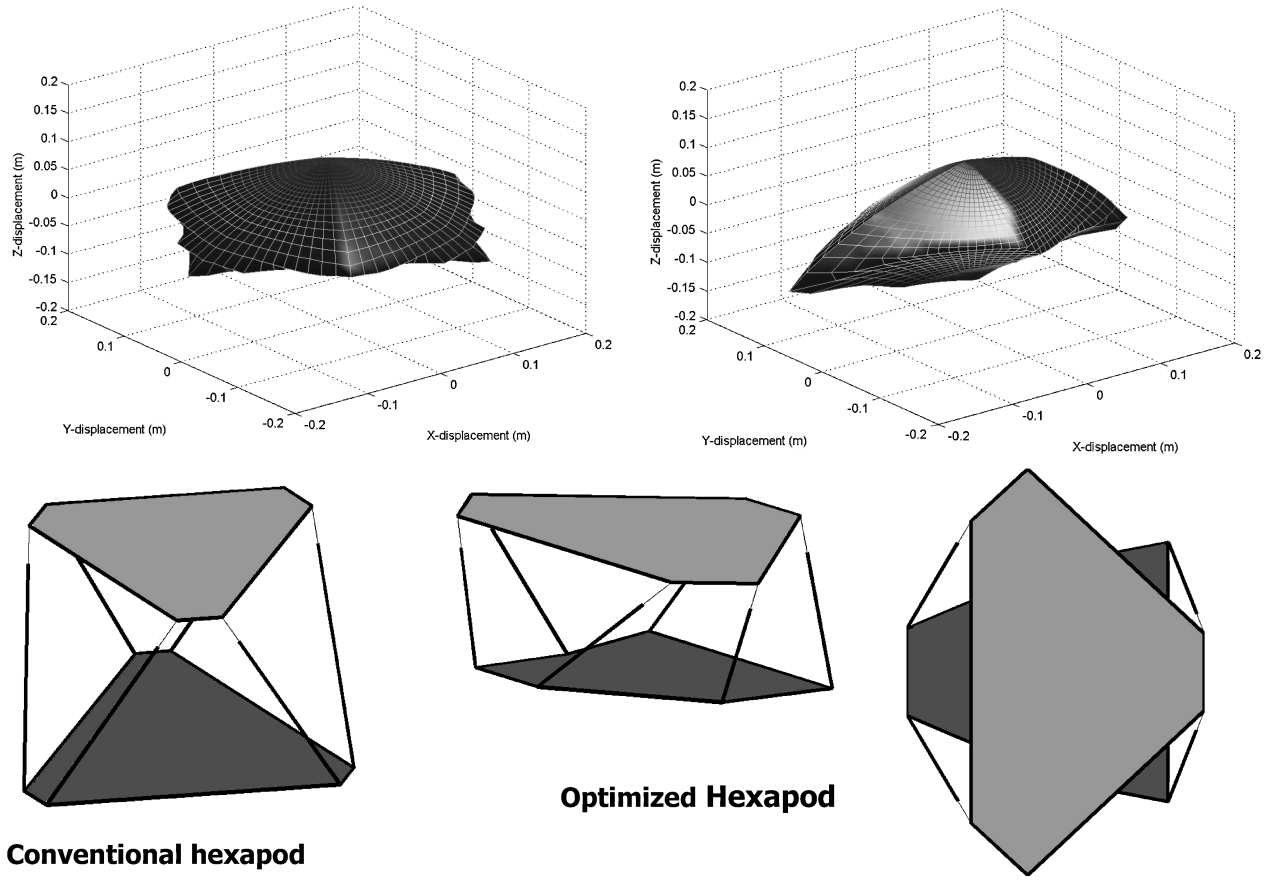

Fig. 13 Work space (translations only shown) and mechanism geometry of a conventional (left) and optimized (right) motion cueing system for the Wright Flyer simulator.

Conclusions

The aforementioned process has demonstrated how one can specify the motion cueing algorithm and geometry of a flight simulator motion base in an objective way. The overall process is shown in Fig. 1. Although the latest scientific knowledge in motion perception and in motion-base design technologies has been applied here, the development of this analytical process is still in progress. The general motion perception model discussed herein must be developed further before it can be fully applied to this type of analysis. Support for further research is required in order to evaluate and fully validate the optimal wash-out filters as demonstrated in this paper. In addition, support is necessary to continue the development of motion perception models. Subsequently, with this perception model the full use of the analysis will make it possible to determine the parameters of the high-pass filters for linear motion as well.

The wash-out filter parameters are adjusted to provide a realistic environment for the feedback of the aircraft dynamics. The prime aim has been to represent the angular accelerations, rates, and positions, which through recent perception research have been shown to have the greatest impact on the skill-based behavior. The onsets (generated within the aircraft math model) are still however passed through the motion drive filters.

The results obtained so far are indeed promising, and work is underway to continue the validation of this process. The main observation so far has been that by making a correct choice of the wash-out parameters the pilot's control behavior can be restored very closely to that in real flight.

The mechanical design proposed in this paper is one unique geometric solution. The emphasis should be clearly the process rather than the design itself. The particular application was initially for a low-cost transportable demonstrator (hence the relatively small motion system). Nonetheless, significant improvements to the desired work space were obtained through the integrated optimization process.

By using a representative set of flight files, the motion system space required for the operation of the intended simulator can be obtained before the motion system is designed. A feedback of the results of the design into the analysis can be used to fine tune the final wash-out algorithm and motion system. The fact remains that this process allows the designer to achieve the most suitable wash-out characteristics and motion system performance, within the capabilities of existing mechanical hardware components. Cost-benefit studies can then be carried out to yield the best solution for the end-user customer.

The approach described here is not only novel but also can introduce significant commercial advantages to flight simulation. By reducing the uncertainty that can result through (current) heuristic optimization, the user can be confident that the simulation closely represents the vehicle characteristics. This can have implications for both training and vehicle development simulators. Secondly, the mechanical design requires only minor changes to the system geometry (for example, slightly longer or shorter actuators, with their end joints locations differing from conventional simulator hexapods). Applications of this approach have shown that significant improvements in the usable work space can result from this approach.

The 1903 Wright Flyer was a highly sensitive flight vehicle, and the capabilities of its developers and pilots are to be commended. Had Wilbur and Orville access to a motion-base simulator designed through techniques as those shown here, perhaps their design process could have been improved.

Although aviation—and flight simulation—have come far since, motion cueing remains an area that needs attention.

Acknowledgments

Gareth Padfield and B. Lawrence of the University of Liverpool are thanked for the provision of Wright Flyer data. Bosch-Rexroth graciously provided motion system data for the optimization example.

References

[1]Howard, F., *Wilbur and Orville—A Biography of the Wright Brothers*, Alfred A. Knopf, New York, 1987, pp. 136, 137.

[2]Teunissen, R., "The Future of Simulation and Training," *Proceedings of the Flight Simulation Conference* "*Can Flight Simulation Do Everything*," Royal Aeronautical Society, London, 1999, pp. 6.1–6.11.

[3]Advani, S. K., and Hosman, R. J. A. W., "Integrated Motion Cueing Algorithm and Motion-Base Design for Flight Simulation," *Proceedings of the Flight Simulation Conference Flight Simulation—The Next Decade*, Royal Aeronautical Society, London, 2000, pp. 24.1–24.9.

[4]Advani, S. K., Giovannetti, D., and Blum, M., "Design of a Hexapod Motion Cueing System for the NASA Ames Vertical Motion Simulator," *AIAA Meeting Papers on Disc* [CD-ROM], Vol. 7, No. 4, AIAA, Reston, VA, 2002.

[5]Hosman, R. J. A. W., Advani, S. K., and Haeck, N., "Integrated Design of Flight Simulator Motion Cueing Systems," *Proceedings of the Flight Simulation Conference Developments in Simulator Systems—Integration and Effectiveness*, Royal Aeronautical Society, London, 2002, pp. 16.1–16.12.

[6]Hosman, R. J. A. W., "Pilots Perception and Control of Aircraft Motion," Ph.D. Dissertation, Dept. of Aerospace Engineering, Delft Univ. of Technology, Delft, The Netherlands, Nov. 1996.

[7]Hosman, R. J. A. W., and Stassen, H. G., "Pilot's Perception in the Control of Aircraft Motions," *Control Engineering Practices*, Vol. 7, No. 11, 1999, pp. 1421–1428.

[8]Hosman, R. J. A. W., "Are Criteria for Motion Cues and Time Delays Possible?" *Proceedings of the AIAA Modeling and Simulation Technologies Conference*, AIAA, Reston, VA, 1999, pp. 68–76.

[9]Rasmussen, J., "Skills, Rules, and Knowledge; Signals, Signs, and Symbols, and Other Distinctions in Human Performance Models," *IEEE Transactions on Systems, Man and Cybernetics*, Vol. SMC-13, No. 3, 1983, pp. 257–266.

[10]Hess, R. A., "A Model for the Human's Use of Motion Cues in Vehicular Control," *Journal of Guidance, Control, and Dynamics*, Vol. 13, No. 2, 1990, pp. 476–482.

[11]Hosman, R. J. A. W., and Mulder, M., "Perception of Flight Information from EFIS Displays," *Control Engineering Practices*, Vol. 5, No. 3, 1997, pp. 383–390.

[12]McRuer, D. T., and Jex, H. R., "A Review of Quasi-Linear Pilot Models," *IEEE Transactions on Human Factors in Electronics*, Vol. HFE-8, No. 3, 1967, pp. 231–249.

[13]Levison, W. H., and Junker, A. M., "A Model for the Pilot's Use of Motion Cues in Steady State Roll-Axis Tracking Tasks." *Proceedings of the AIAA Flight Simulation Technologies Conference*, AIAA, New York, 1978, pp. 149–159.

[14]Hess, R. A., "Feedback Control Models," *Handbook of Human Factors*, edited by G. Salvendy, Wiley-Interscience, New York, 1985, Chap. 9.5.

[15]Bos, J. E., Bles, W., and Hosman, R. J. A. W., "Modeling Human Spatial Orientation and Motion Perception," *AIAA Meeting Papers on Disc* [CD-ROM], Vol. 6, No. 4, AIAA, Reston, VA, 2001.

[16]Stewart, D., "A Platform with Six-Degrees-of-Freedom," *Proceedings of the Institute of Mechanical Engineers*, Vol. 180, Pt. 1, No. 5, 1965–1966, pp. 371–386.

[17]Advani, S. K., "The Kinematic Design of Flight Simulator Motion-Bases," Ph.D. Dissertation, Dept. of Aerospace Engineering, Delft Univ. of Technology, Delft, The Netherlands, 1998.

[18]Advani, S. K., Nahon, M., and Haeck, N., "Optimisation of Six-Degrees-of-Freedom Flight Simulator Motion Systems," *Journal of Aircraft*, Vol. 36, No. 5, 1999, pp. 753–763.

[19]Culick, F. E. C., "What the Wright Brothers Did and Did Not Understand About Flight Mechanics—In Modern Terms," *AIAA Meeting Papers on Disc* [CD-ROM], Vol. 6, No. 4, AIAA, Reston, VA, 2001.

[20]Lawrence, B., and Padfield, G. D., "A Handling Qualities Analysis of the Wright Brothers' 1902 Glider," *AIAA Meeting Papers on Disc* [CD-ROM], AIAA, Reston, VA, 2003.

[21]Jex, H. R., Magdaleno, R. E., and Lee, D., "Virtual Reality Simulation of the '03 Wright Flyer Using Full-Scale Test Data," AIAA Paper 2000-4088, Aug. 2000.

[22]Reid, L. D., and Nahon, M. A., "Flight Simulation Motion-Base Drive Algorithms: Part 2—Selecting the System Parameters," Univ. of Toronto, Rept. 307, Toronto, May 1986.